

Structure and magnetic properties of RAlSi (R=light rare earth)

Tai Wang(王泰), Yongquan Guo(郭永权), and Cong Wang(王聪)
Citation: Chin. Phys. B, 2021, 30 (**7**): 075102. DOI: 10.1088/1674-1056/abe3e8
Journal homepage: http://cpb.iphy.ac.cn; http://iopscience.iop.org/cpb

What follows is a list of articles you may be interested in

Powder x-ray diffraction and Rietveld analysis of $(C_2H_5NH_3)_2CuCl_4$

Yi Liu(刘义), Jun Shen(沈俊), Zunming Lu(卢遵铭), Baogen Shen(沈保根), and Liqin Yan(闫丽琴)
Chin. Phys. B, 2021, 30 (**6**): 067502. DOI: 10.1088/1674-1056/abee0a

Electronic shell study of prolate Li_n(n =**15**-17) clusters: Magnetic superatomic molecules

Lijuan Yan(闫丽娟), Jianmei Shao(邵健梅), and Yongqiang Li(李永强)
Chin. Phys. B, 2020, 29 (**12**): 125101. DOI: 10.1088/1674-1056/abb669

Crystal structure and electromagnetic responses of tetragonal GdAlGe

Cong Wang(王聪), Yong-Quan Guo(郭永权), Tai Wang(王泰), and Shuo-Wang Yang(杨硕望)
Chin. Phys. B, 2020, 29 (**12**): 127502. DOI: 10.1088/1674-1056/abad25

Critical behavior in the layered organic-inorganic hybrid $(CH_3NH_3)_2CuCl_4$

Tina Raoufi, Yinina Ma(马怡妮娜), Young Sun(孙阳)
Chin. Phys. B, 2020, 29 (**6**): 067503. DOI: 10.1088/1674-1056/ab892c

Study on the electromagnetic propertiesof a coated radar absorbent

Zhang Shuan-Qin
Chin. Phys. B, 2012, 21 (**6**): 065101. DOI: 10.1088/1674-1056/21/6/065101

Structure and magnetic properties of RAlSi (R = light rare earth)*

Tai Wang(王泰), Yongquan Guo(郭永权)†, and Cong Wang(王聪)

School of Energy Power and Mechanical Engineering, North China Electric Power University, Beijing 102206, *China*

(Received 8 December 2020; revised manuscript received 4 February 2021; accepted manuscript online 7 February 2021)

We prepared the semimetals RAlSi (R = light rare earth), and systematically study their crystal structures and magnetic properties. X-ray diffractions confirm the coexistence of the site-disordered phase with group space of $I4_1/amd$ and the noncentrosymmetrically ordered phase with space group of $I4_1md$ in RAlSi alloy. The ordered phase is the main phase in RAlSi alloy. RAlSi alloys show nonmagnetic character for R = La, low temperature ferromagnetic order for R = Ce, Pr, and paramagnetic character for R = Nd, respectively. SmAlSi shows metamagnetic transition at 10 K and ferromagnetic order at 143 K, respectively. SmAlSi follows the van Vleck paramagnetic model in its paramagnetic region. The magnetization curves of RAlSi (R = Ce, Pr, Sm) follow the mixed model of ferromagnetism and paramagnetism, and the fitted saturation moment M_S depends on the moment of trivalent rare earth. The paramagnetic susceptibility χ of RAlSi is going up with increasing the atomic order numbers of rare earth elements. This reveals that the magnetic property of RAlSi originates from the rare earth.

Keywords: RAlSi, crystal structure, magnetic properties

PACS: 51.60.+a, 75.50.–y, 75.47.–m **DOI:** 10.1088/1674-1056/abe3e8

1. Introduction

The topologically electronic and strongly spin-orbit coupling materials have been systematically investigated and their unique characteristics have been revealed so far.[1–14] Weyl semimetals have received great attention due to their unusual characters of space-inversion symmetry breaking for type I or time-reversal symmetry breaking for type Ⅱ.[1,5,8,10,12] Type-I Weyl semimetals have been realized experimentally in TaAs and its isostructural materials such as TaP, NbAs, and NbP.[5,6,8,9] Though it is difficult to identify the magnetic Weyl semimetals with type Ⅱ by utilizing the angle resolved photo emission spectroscopic (ARPES) measurement, the unique properties of type-Ⅱ Weyl semimetals have been experimentally verified by magnetic and electric measurements for some intermetallic compounds such as $HgCr_2Se_4$,[14] RAlGe (R = La, Ce, Pr),[11,15–17] $SrMnSb_2$,[10] and Mn_3Z (Z = Ga, Sn, Ge).[18,19] The significant coupling of magnetic configurations to semi-metallic electronic structure in magnetic Weyl semimetal may provide technologically useful behavior for sensors and spintronic devices.[20,21]

In recent years, the ternary RAlGe (R = La, Ce and Pr) intermetallics have attracted considerable attention as potential candidates of Weyl semimetals.[11,15–17,21–23] The body tetragonal RAlGe (R = rare earth) with space group $I4_1md$ are firstly predicted to have either type-I or type-Ⅱ Weyl fermions, depending primarily on the radius of rare earth.[23] The light rare earth based RAlGe (R = La, Ce, Pr) have been experimentally studied.[11,15–17,21–23] LaAlGe and CeAlGe belong to the type-Ⅱ Weyl semimetals.[22,23] CeAlGe exhibits ferromagnetic characteristics with strong magnetic anisotropy along the crystallographic a axis and its angular magnetoresistance response exceeds 1000% rad^{-1} along the high symmetry axis within 1°.[11,21] PrAlGe presents the ferromagnetic characteristics along the easy c axis. A large anomalous Hall conductivity of 680 $\Omega^{-1}\cdot cm^{-1}$ has been observed, which may be due to the contribution of intrinsic Berry-phase Karplus–Luttinger mechanism.[15] NdAlGe shows the spin-glass-like characteristics at low temperature and van Vleck paramagnetism in high temperature region, respectively.[24] The tetragonal GdAlGe orders ferromagnetically at 21 K, and its magnetic properties are strongly related to its special magnetic structure formed by magnetic Gd3 isosceles triangles. The ferromagnetism may originate from the exchange interaction between two parallel Gd3 isosceles triangles.[25]

Recently, the interest has been extended to the isomorphous RAlSi family. $PrAlGe_{1-x}Si_x$ is revealed with a transition of the anomalous Hall effect from an intrinsic (x below 0.5) to an extrinsic region (x higher than 0.5).[26] CeAlSi is a new type of ferromagnetic Weyl semimetal, which shows novel anisotropic anomalous Hall responses along the easy and hard axes.[27] The ferromagnetic PrAlSi has a huge anomalous Hall conductivity of ∼2000 $\Omega^{-1}\cdot cm^{-1}$.[28] The crystal structure of CeAlSi is initially reported as site-disordered $I4_1/amd$.[29–31] However, the later studies show that the noncentrosymmetrically ordered structure with a space group of $I4_1md$ is preferred,[26] which is an isostructure of CeAlGe.[11,16,21] The same question arises for the preferred structural model in the other RAlSi alloys. Accord-

*Project supported by the Fundamental Research Funds for the Central Universities of China (Grant No. 2019QN085).

†Corresponding author. E-mail: yqguo@ncepu.edu.cn

© 2021 Chinese Physical Society and IOP Publishing Ltd

ing to the international center of diffraction database (ICDD), the crystal structures of RAlSi (R = light rare earth) are the noncentrosymmetric with space group of $I4_1md$ for R = Ce and Sm; site-disordered $I4_1/amd$ for NdAlSi, respectively. However, no record is available for equiatomic LaAlSi and PrAlSi, which may be considered as $RSi_{2-x}Al_x$ solid solution with $x = 1$. $RSi_{2-x}Al_x$ solid solutions crystallize in body centered tetragonal α-$ThSi_2$ type structure with a space group of $I4_1/amd$, where Al and Si occupy randomly the 8*e* crystal position.[29,32,33] However, the recent study shows that the equliatomic PrAlSi not only fits the site-disordered α-$ThSi_2$ type structure but also the noncentrosymmetrically ordered $I4_1md$ as well. The minor difference between the two models is the temperature factor.[28] Thus, in order to determine the structural models of equiatomic RAlSi (R = light rare earth), the interest has been focused on the crystal structure and magnetic properties of RAlSi in this study.

2. Material and methods

The nominal composition of RAlSi (R = light rare-earth element) were prepared using arc melting under an argon gas atmosphere and vacuum solid state reaction technology. The purities of raw materials are more than 99.99 wt%. Each sample was remelted four times for its homogeneity. The vacuum annealing process, which could remove the potential metastable phase and residual stress in samples, was carried out at 1023 K for seven days in the vacuum evacuated quartz tube. The crystal structures of RAlSi (R = light rare-earth element) were measured using a Rigaku G/max 2500 x-ray diffractometer with Cu $K_{\alpha 1}$ radiation ($\lambda = 1.54056$ Å). The surface morphologies and element components of RAlSi (R = light rare-earth element) were recorded with the field emission scanning electron microscopy (SEM) equipped with energy dispersive spectra (EDS). The applied field dependence of magnetization (*M*–*H*) and temperature dependence of magnetization (*M*–*T*) of RAlSi alloys were measured using a superconducting quantum interference device (SQUID). *M*–*T* curves were measured in the temperature range of 2 to 300 K with an external field of 50 Oe for CeAlSi and PrAlSi, and in the temperature range from 5 to 300 K with an external field of 1 kOe for NdAlSi and SmAlSi, respectively. *M*–*H* curves of RAlSi alloys were measured in applied fields ranging from 0 to 50 kOe at various temperatures.

3. Results and discussion

In order to determine the crystal structures of equiatomic light rare earth based RAlSi, the three possible structural models, which correspond to the site-disordered $I4_1/amd$, noncentrosymmetrically ordered $I4_1md$ and their mixed model, are used for Rietveld structural refinement. The refinement results show that the x-ray diffraction patterns of RAlSi prefer to follow the mixed model, the residual pattern factor R_p and residual weight pattern factor R_{wp} are the smallest among the three models. NdAlSi is selected as a typical example, and its x-ray diffraction patterns are refined with the above-mentioned three possible structural models, as shown in Figs. 1(a)–1(c). The difference between site-disordered $I4_1/amd$ and noncentrosymmetrically ordered $I4_1md$ is small. R_p and R_{wp} are corresponding to 12.352% and 16.355% for $I4_1md$; 12.404% and 16.389% for $I4_1/amd$. However, the x-ray patterns of NdAlSi fit the mixed model very well. R_p and R_{wp} decrease to 9.235% and 12.951%, implying that this structural model is acceptable.

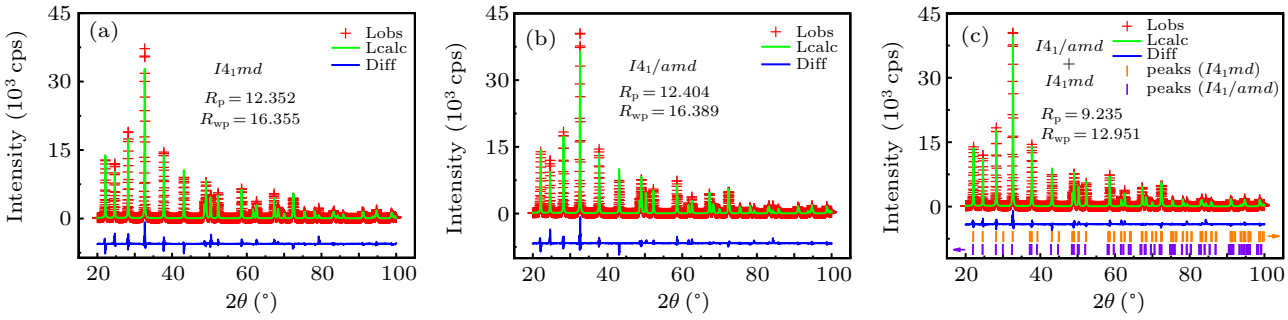


Fig. 1. The refined x-ray diffraction patterns of NdAlSi based on the noncetrosymmetrically ordered $I4_1md$ model (a), the site-disordered $I4_1/amd$ model (b), and the mixed model (c) of $I4_1md$ and $I4_1/amd$.

The refinement shows that the lattice parameters of the disordered phase is slightly larger than those of the ordered phase. It reveals that the peak separation is necessary for the widened diffraction peaks caused by overlaps of diffraction peaks for the two phases. The refined x-ray diffraction patterns of RAlSi are shown in Figs. 2(a)–2(e). The red symbols of + and green lines denote the observed and calculated x-ray diffraction patterns of RAlSi. The intensity differences between the observed and calculated x-ray diffractions are shown in the lowest line. The orange and violet vertical bars represent the peak positions of $I4_1md$ and $I4_1/amd$ phases, respectively. It is significant that diffraction peak positions of

$I4_1/amd$ phase shift to the low angle compared to those of $I4_1md$ phase. This phenomenon is ascribed to the increase of lattice parameter for site-disordered $I4_1/amd$ phase, induced by the different occupations of Al and Si atoms in two structures. The lattice parameters of RAlSi decrease with increasing the atomic order number of rare earth element due to the lanthanide contraction effect.

The weight proportion of two phases in RAlSi alloys can be estimated by the following equation:[34]

$$W = \frac{S_i A_i V_i Z_i}{\sum_i S_i A_i V_I Z_i}, \tag{1}$$

where S_i, A_i, V_i, Z_i are the scale factor, molecular weight, cell volume and numbers of molecular in unit cell for the ith phase, respectively. The calculations of phase contents reveal that the noncentrosymmetrically ordered phase is the main phase in RAlSi alloy. Table 1 lists the refined structural parameters and phase weight proportions in RAlSi alloys.

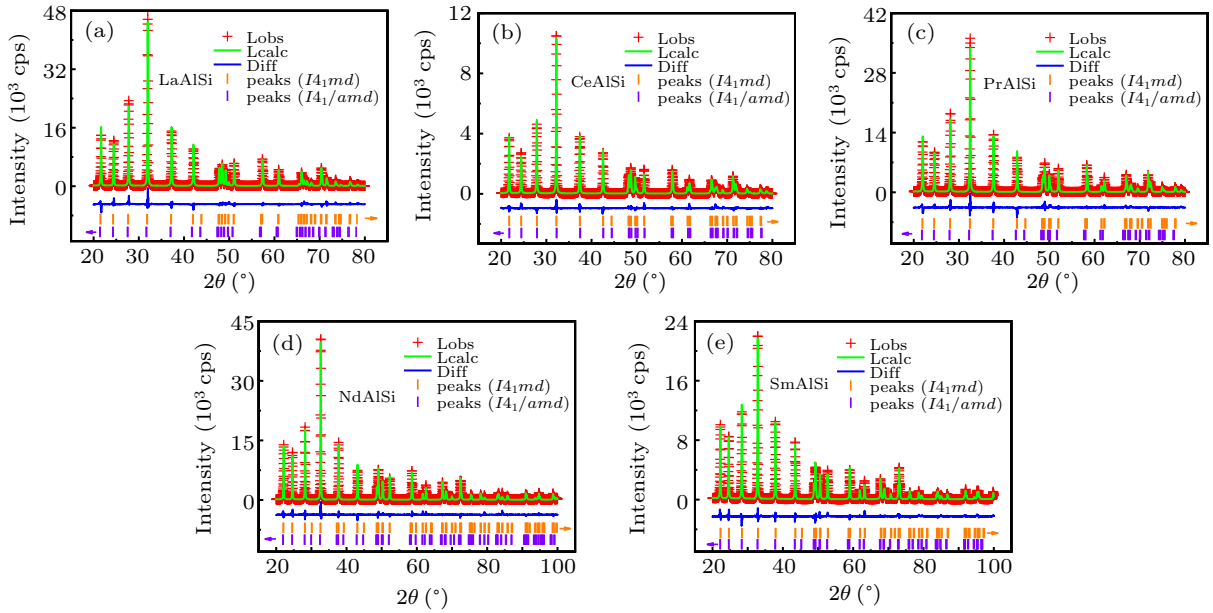


Fig. 2. The refined and observed XRD patterns of RAlSi.

Table 1. The refined phase structural parameters of RAlSi with structural models of $I4_1md$ and $I4_1/amd$.

		LaAlSi	CeAlSi	PrAlSi	NdAlSi	SmAlSi
$I4_1md$ phase	a (Å)	4.3069	4.2502	4.2525	4.2010	4.1566
	c (Å)	14.6494	14.5769	14.5743	14.5079	14.4552
	R (4a)	(0,0,0.57515)	(0,0,0.58924)	(0,0,0.57618)	(0,0,0.57802)	(0,0,0.57744)
	Al (4a)	(0,0,0.16793)	(0,0,0.16902)	(0,0,0.16541)	(0,0,0.16227)	(0,0,0.16602)
	Si (4a)	(0,0,0)	(0,0,0)	(0,0,0)	(0,0,0)	(0,0,0)
$I4_1/amd$ phase	a (Å)	4.3299	4.2462	4.2480	4.2230	4.1733
	c (Å)	14.6767	14.5521	14.5705	14.5235	14.4784
	Al/Si (8e)	(0,0.25,0.30298)	(0,0.25,0.30282)	(0,0.25,0.30190)	(0,0.25,0.28313)	(0,0.25,0.31496)
	R (4a)	(0,0.75,0.125)	(0,0.75,0.125)	(0,0.75,0.125)	(0,0.75,0.125)	(0,0.75,0.125)
R_p		9.547	8.647	9.622	9.235	8.666
R_{wp}		12.876	12.460	12.563	12.951	11.647
Percentage of $I4_1md$ phase		0.9652	0.7800	0.9568	0.9467	0.8773
Percentage of $I4_1/amd$ phase		0.0348	0.2200	0.0432	0.0533	0.1227

SEM morphologies and EDS spectra of RAlSi (R = light rare-earth element) powders are displayed in Figs. 3(a)–3(e). The grain growths exhibit inhomogeneity from large bulks to small pieces with sizes ranging from 0.5 μm to 7 μm, the small grains distribute on the surface of the large ones, and the grains tend to agglomerate with increasing the atomic order number of rare earth element. EDS measurements show that the element compositions of RAlSi alloys are close to the ratio of 1:1:1 as the stoichiometrically equiatomic RAlSi, and the slight deviation from the normal structural formula may be ascribed to the volatilization during the melting process.

Figures 4–7 show that the temperature dependence of magnetizations (M–T) curves of RAlSi alloys measured with field-cooled (FC) and zero-field-cooled (ZFC). CeAlSi is ferromagnetic, as shown in Fig. 4, which ascribes to the interaction between the local f-moments of Ce^{3+} and the non-

centrosymmetric lattice.[27] Curie temperature of CeAlSi is 7.7 K, which is close to that of $CeAl_{0.9}Si_{1.1}$.[35]

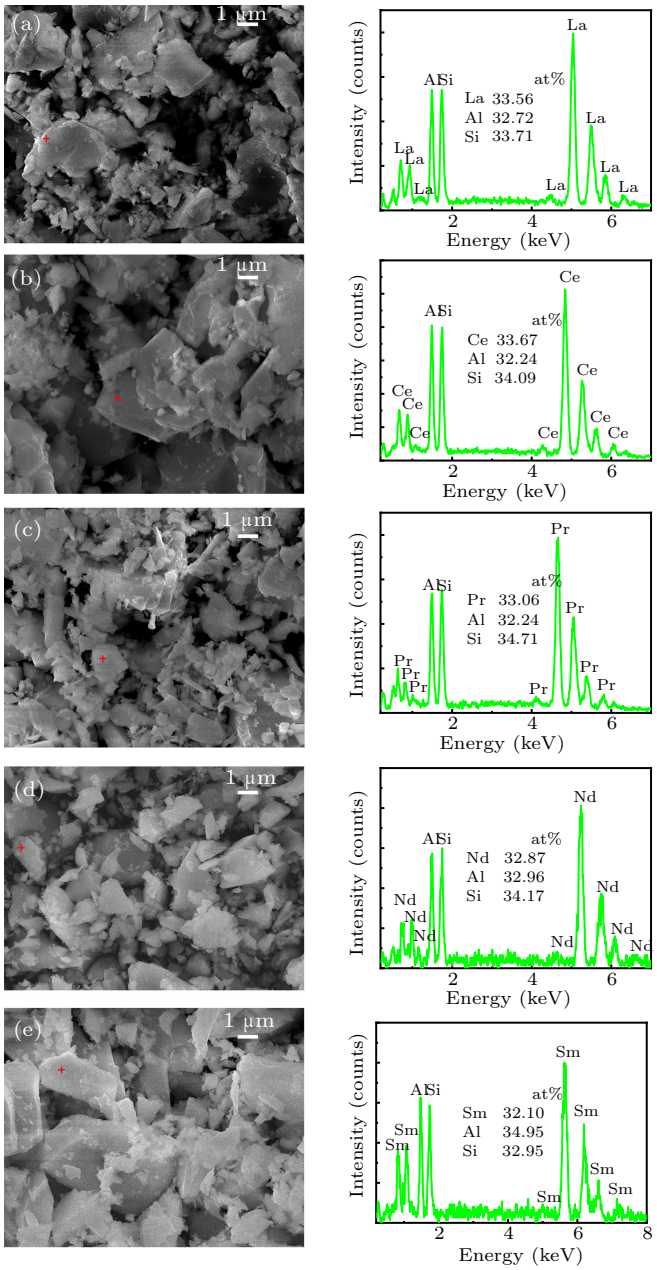


Fig. 3. SEM morphologies and EDS patterns of RAlSi: (a) for LaAlSi, (b) for CeAlSi, (c) for PrAlSi, (d) for NdAlSi, and (e) for SmAlSi.

Figure 5 shows that PrAlSi orders ferromagnetically at 17.7 K, its Curie temperature is very close to the previously reported $T_C = 17.2$ K.[26] The cusp-like transitions are observed at 5.2 K for CeAlSi and 16.5 K for PrAlSi. The remarkable difference between ZFC and FC curves suggests that the cusp-like transition may be due to the spin-glass-like phenomenon, which is similar to the thermal irreversibility $\chi(T)$ for RAlX (R = Ce, Pr; X = Ge, Si) in the temperature region of $T < T_C$.[15–17,26,28,36] However, the M–T curve of NdAlSi shows only paramagnetic characteristics as shown in Fig. 6. SmAlSi shows complex magnetic properties. According to the FC curve in Fig. 7, SmAlSi shows metamagnetic transition at 10 K and weak ferromagnetic-paramagnetic transition at 143 K. However, the ZFC curve shows an extra magnetic transition at 60 K, which may be due to the disordered arrangement of Sm moment. In addition, the unconventional fluctuations may be due to the heavy-fermion effect in temperature ranges from 50 to 80 K, which is possibly caused by the unconventional magnetic ordering of the involvement of multiple 4f elections of Sm ions in the hybridization process.[37]

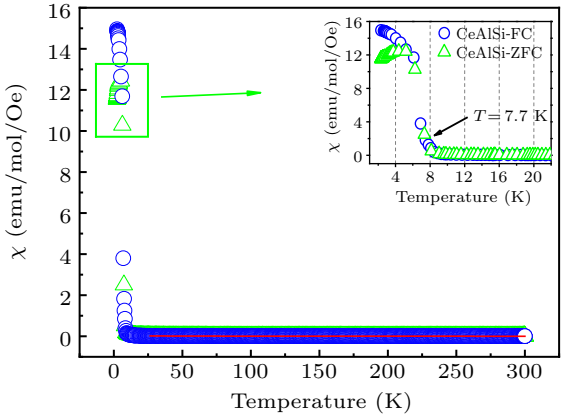


Fig. 4. The temperature dependence of magnetization (M–T) for CeAlSi, and the fitted M–T curve based on Curie–Weiss law in paramagnetic region. Inset: the ferromagnetic transition.

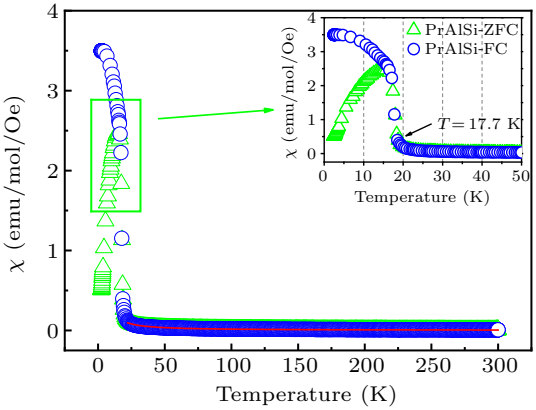


Fig. 5. The temperature dependence of magnetization (M–T) for PrAlSi, nd the fitted M–T curve based on Curie–Weiss law in paramagnetic region. Inset: the magnetic transition.

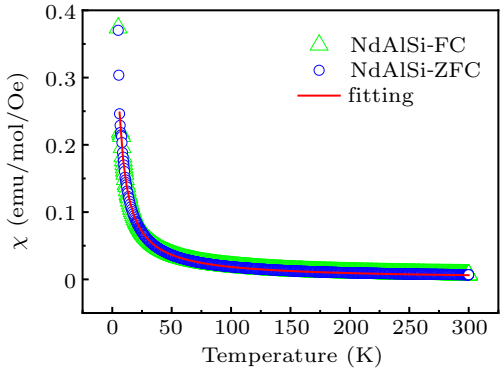


Fig. 6. The observed and fitted M–T curves based on Curie–Weiss law of NdAlSi.

The χ–T curves of RAlSi (R = Ce, Pr, Nd) follow the Curie–Weiss law in their paramagnetic region. The fitted

curves are shown in Figs. 4, 5, and 6 for CeAlSi, PrAlSi, and NdAlSi, respectively. The fitted Curie–Weiss temperature θ_P is corresponding to -24.33 K for CeAlSi, 5.56 K for PrAlSi, and -8.75 K for NdAlSi. The negative θ_P implies the possible antiferromagnetic order in NdAlSi. However, the antiferromagnetism is not experimentally observed in NdAlSi alloy.

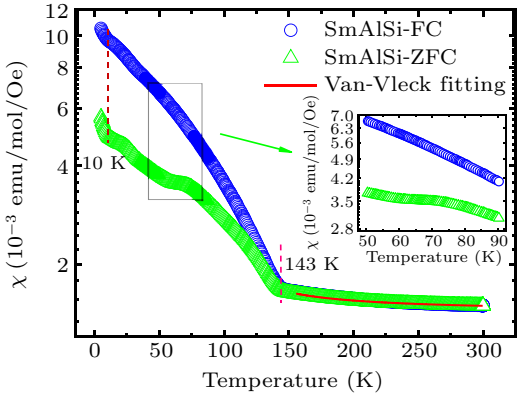


Fig. 7. The temperature dependence of magnetization for SmAlSi, and the fitting M–T curve based on the van Vleck law in paramagnetic region.

The effective moment μ_{eff} is estimated with the equation $N\mu_{\text{eff}}^2 = 3CMK_B$, where C, M, K_B, N correspond to the Curie–Weiss constant, the molecular weight, the Boltzmann constant and the number of atoms.[38] The calculated μ_{eff}'s are 2.53 μ_B for CeAlSi, 3.56 μ_B for PrAlSi and 3.79 μ_B for NdAlSi. The effective moments of paramagnetic CeAlSi, PrAlSi and NdAlSi are close to the moments of trivalent Ce^{3+} (2.54 μ_B), Pr^{3+} (3.58 μ_B) and Nd^{3+}(3.62 μ_B). This reveals that the contribution to moment originates from rare earth in RAlSi.

The temperature dependence of susceptibility for SmAlSi does not fit the Curie–Weiss law in the paramagnetic region. The surplus molar magnetic susceptibility most likely comes from a typical behavior of Sm^{3+} ions, which ascribe to the different multiplets between $J = 5/2$ (ground state) and $J = 7/2$ (first excited state).[39–43] In the paramagnetic region, the susceptibility of SmAlSi follows the modified van Vleck paramagnetic mode with an equation of $\chi = \chi_0 + C/(T - \theta_P)$.[44,45] The effective magnetic moment is 0.329 μ_B, which is smaller than the moment of Sm^{3+} (0.85 μ_B). Such a reduction reveals a pronounced crystal field effect in SmAlSi.[39,44,45] The small positive value of θ_P indicates dominant ferromagnetic interactions for the magnetism of SmAlSi.[39]

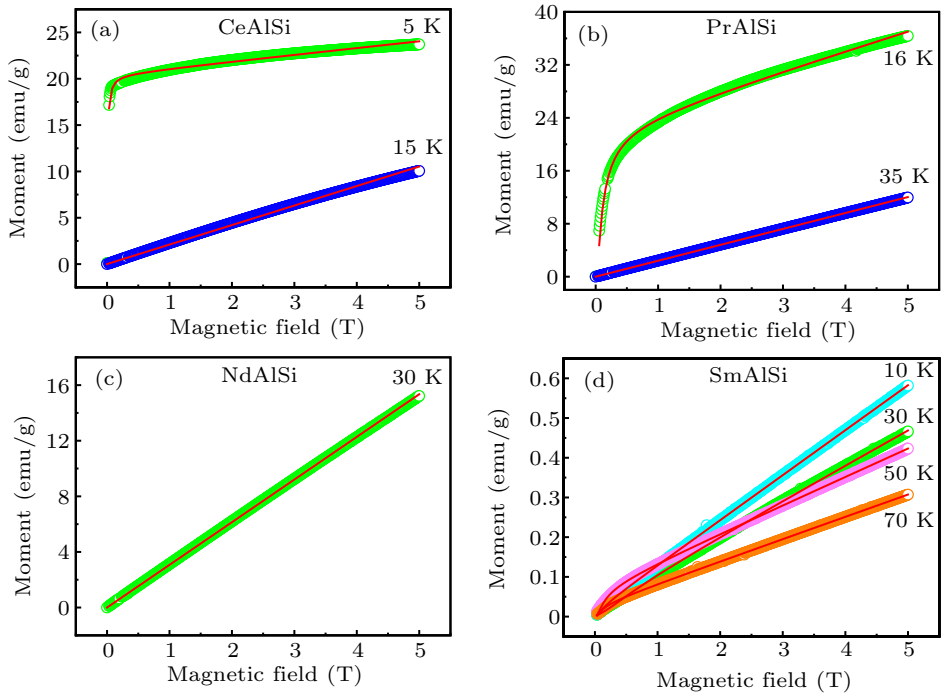


Fig. 8. The observed and fitted field dependences of magnetizations for RAlSi: (a) for CeAlSi, (b) for PrAlSi, (c) for NdAlSi and (d) for SmAlSi.

Figure 8 shows that RAlSi (R = Ce, Pr, Sm) exhibit mixture of ferromagnetism and paramagnetism, however, NdAlSi presents only the paramagnetic character. In paramagnetic region, the magnetizing curves for RAlSi follow a linear equation as follows:

$$M = \chi H, \tag{2}$$

where H and χ are the external field and susceptibility, respectively.

The field dependence of magnetization curves for the RAlSi alloys follows the mixture magnetism model as follows:[46,47]

$$M = M_S \cdot \exp\left(-\frac{a}{H}\right) + \chi H. \tag{3}$$

The first term originates from the contribution of ferromagnetic phase, which is based on the Langevin model,[48] and the second term contributes to magnetization originating from

the paramagnetic phase, where M_s and χ are the saturation moment and susceptibility, respectively.

The fitted and observed magnetization curves for RAlSi are marked with circles and solid lines as shown in Fig. 8, respectively. Table 2 lists the fitted parameters of PrAlSi and NdAlSi in the paramagnetic region. The paramagnetic susceptibility χ of RAlSi is enhanced with increasing the atomic order number of rare earth elements from Ce to Nd, which may be due to the increasing moment of trivalent rare earth ions. Table 3 lists the fitted parameters of RAlSi (R = Ce, Pr, Sm) alloys based on the mixture model of ferromagnetism and paramagnetism. For ferromagnetic RAlSi (R = Ce, Pr), the saturation moment of PrAlSi is larger than that of CeAlSi, which is due to the large moment of trivalent Nd compared to that of Ce^{3+}. Thus, it implies that the saturation moment M_S depends on the moment of trivalent rare earth. With increasing temperature, the fitted M_S of CeAlSi shows an opposite tendency with its susceptibility χ. M_s is going down, whereas the susceptibility χ is going up. The susceptibility of SmAlSi shows a decreasing tendency with increasing temperature, which may be due to its various magnetic transitions.

Table 2. The fitted parameters of RAlSi (R = Ce, Pr, Nd) in their paramagnetic regions.

Parameters	$M = \chi H$	
Compounds	PrAlSi 35 K	NdAlSi 30 K
Reduced χ^2	9.5307×10^{-4}	0.0034
Adjusted R^2	0.99992	0.99982
χ (emu/g·kOe)	2.40591	3.06891
Standard error of χ (emu/g·kOe)	4.3641×10^{-4}	8.3263×10^{-4}

Table 3. The fitting parameters of RAlSi (R = Ce, Pr, Sm) with the mixed model of ferromagnetism and paramagnetism at various temperatures.

Parameters	$M = M_S \cdot \exp(-a/H) + \chi H$						
Compounds	CeAlSi		PrAlSi	SmAlSi			
	5 K	15 K	16 K	10 K	30 K	50 K	70 K
Reduced χ^2	0.03695	0.0026	0.1548	5.336×10^{-7}	3.525×10^{-6}	1.512×10^{-6}	2.644×10^{-7}
Adjusted R^2	0.9841	0.9999	0.9957	0.9999	0.9998	0.9999	0.9999
Values:							
M_S (emu/g)	20.4342	1.6228	22.7781	0.01771	0.03495	0.06945	0.02802
a (kOe)	0.00651	1.12465	0.09123	0.1351	0.77448	0.13965	0.1163
χ (emu/g·kOe)	0.72686	1.77590	2.92897	0.11308	0.08776	0.07113	0.05599
Standard error:							
M_S (emu/g)	0.01982	0.03549	0.0588	1.238×10^{-4}	9.314×10^{-4}	2.085×10^{-4}	8.179×10^{-5}
a (kOe)	1.993×10^{-4}	0.01765	0.00113	0.00346	0.02118	0.00147	0.00132
χ (emu/g·kOe)	0.00626	0.0057	0.01607	3.216×10^{-5}	1.671×10^{-4}	5.424×10^{-5}	2.182×10^{-5}

4. Conclusion

RAlSi (R = light rare earth) alloys consist of two phases according to x-ray diffraction, which are corresponding to the site-disordered phase with group space of $I4_1/amd$ and the noncentrosymmetrically ordered phase with space group of $I4_1md$. The ordered phase is the main phase in RAlSi alloy. RAlSi alloys show nonmagnetic character for R = La, low temperature ferromagnetic order for R = Ce, Pr, and paramagnetic character for R = Nd, respectively. SmAlSi shows metamagnetic transition at 10 K and weak ferromagnetic order at 143 K, respectively. RAlSi (R = Ce, Pr, Nd) follow the normal Curie–Weiss law in their paramagnetic regions, however, SmAlSi follows the van Vleck paramagnetic model. In the paramagnetic region, the susceptibilities of RAlSi are enhanced with increasing the atomic order number of rare earth element. The magnetization curves of RAlSi (R = Ce, Pr, Sm) follow the mixed model of ferromagnetism and paramagnetism. The fitted M_S depends on the moment of trivalent rare earth. For ferromagnetic RAlSi (R = Ce, Pr), the M_S of PrAlSi is larger than that of CeAlSi. With increasing temperature, the fitted M_S of CeAlSi shows an opposite tendency with its susceptibility χ. M_s is going down, whereas the susceptibility χ is going up. The susceptibility of SmAlSi shows a decreasing tendency with increasing temperature. This may be due to its various magnetic transitions. The studies reveal that the magnetic property of RAlSi originates from the rare earth.

References

[1] Weng H, Fang C, Fang Z, Bernevig B A and Dai X 2015 *Phys. Rev. X* **5** 011029

[2] Xu S Y, Belopolski I, Alidoust N, Neupane M, Bian G, Zhang C, Sankar R, Chang G, Yuan Z, Lee C C, Huang S M, Zheng H, Ma J, Sanchez D, Wang B, Bansil A, Chou F, Shibayev P, Lin H and Hasan M Z 2015 *Science* **349** 613

[3] Hasan M Z, Xu S Y, Belopolski I and Huang S M 2017 *Annu. Rev. Condens. Matter Phys.* **8** 289

[4] Li H, He H, Lu H, Zhang H, Liu H, Ma R, Fan Z, Shen S and Wang J 2016 *Nat. Commun.* **7** 10301

[5] Buckeridge J, Jevdokimovs D, Catlow C R A and Sokol A A 2016 *Phys. Rev. B* **93** 125205

[6] Huang S M, Xu S Y, Belopolski I, Lee C C, Chang G, Wang B, Alidoust N, Bian G, Neupane M, Zhang C, Jia S, Bansil A, Lin H and Hasan M Z 2015 *Nat. Commun.* **6** 7373

[7] Jiang W, Huang H, Liu F, Wang J P and Low T 2020 *Phys. Rev. B* **101** 121113

[8] Niemann A C, Gooth J, Wu S C, Baessler S, Sergelius P, Huehne R, Rellinghaus B, Shekhar C, Suess V, Schmidt M, Felser C, Yan B and Nielsch K 2017 *Sci. Rep.* **7** 43394

[9] Lv B, Xu N, Weng H, Ma J, Richard P, Huang X, Zhao L, Chen G, Matt C, Bisti F, Strocov V, Mesot J, Fang Z, Dai X, Qian T, Shi M and Ding H 2015 *Nat. Phys.* **11** 724

[10] Qiu Z, Liao Z and Qiu X 2019 *Chin. Phys. B* **28** 47801
[11] Hodovanets H, Eckberg C J, Zavalij P Y, Kim H, Lin W C, Zic M, Campbe D J, Higgins J S and Paglione J 2018 *Phys. Rev. B* **98** 245132
[12] Xie B, Liu H, Cheng H, Liu Z, Chen S and Tian J 2019 *Phys. Rev. Lett.* **122** 104302
[13] Wang G, Sun Z, Si X and Jia S 2020 *Chin. Phys. B* **29** 077503
[14] Xu G, Weng H M, Wang Z J, Dai X and Fang Z 2011 *Phys. Rev. Lett.* **107** 186806
[15] Meng B, Wu H, Qiu Y, Wang C, Liu Y, Xia Z, Yuan S, Chang H and Tian Z 2019 *APL Mater.* **7** 051110
[16] Puphal P, Mielke C, Kumar N, Soh Y, Shang T, Medarde M, White J S and Pomjakushina E 2019 *Phys. Rev. Mater.* **3** 024204
[17] Puphal P, Pomjakushin V, Kanazawa N, Ukleev V, Gawryluk D J, Ma J, Naamneh M, Plumb N C, Keller L, Cubitt R, Pomjakushina E and White J S 2020 *Phys. Rev. Lett.* **124** 017202
[18] Nakatsuji S, Kiyohara N and Higo T 2015 *Nature* **527** 212
[19] Kuroda K, Tomita T, Suzuki M T, Bareille C, Nugroho A A, Goswami P, Ochi M, Ikhlas M, Nakayama M, Akebi S, Noguchi R, Ishii R, Inami N, Ono K, Kumigashira H, Varykhalov A, Muro T, Koretsune T, Arita R, Shin S, Kondo T and Nakatsuji S 2017 *Nat. Mater.* **16** 1090
[20] Žutić I, Fabian J and Das Sarma S 2004 *Rev. Mod. Phys.* **76** 323
[21] Suzuki T, Savary L, Liu J P, Lynn J W, Balents L and Checkelsky J G 2019 *Science* **365** 377
[22] Xu S Y, Alidoust N, Chang G, Lu H, Singh B, Belopolski I, Sanchez D S, Zhang X, Bian G, Zheng H, Husanu M-A, Bian Y, Huang S M, Hsu C H, Chang T R, Jeng H T, Bansil A, Neupert T, Strocov V N, Lin H, Jia S and Hasan M Z 2017 *Sci. Adv.* **3** e1603266
[23] Chang G, Singh B, Xu S Y, Bian G, Huang S M, Hsu C H, Belopolski I, Alidoust N, Sanchez D S, Zheng H, Lu H, Zhang X, Bian Y, Chang T R, Jeng H T, Bansil A, Hsu H, Jia S, Neupert T, Lin H and Hasan M Z 2018 *Phys. Rev. B* **97** 041104
[24] Wang T, Guo Y, Wang C and Yang S 2020 *Solid State Commun.* **321** 114041
[25] Wang C, Guo Y Q, Wang T and Yang S W 2020 *Chin. Phys. B* **29** 127502
[26] Yang H Y, Singh B, Lu B, Huang C Y, Bahrami F, Chiu W C, Graf D, Huang S M, Wang B, Lin H, Torchinsky D, Bansil A and Tafti F 2020 *APL Mater.* **8** 011111
[27] Yang H Y, Singh B, Gaudet J, Lu B, Huang C Y, Chiu W C, Huang S M, Wang B, Bahrami F, Xu B, Franklin J, Sochnikov I, Graf D E, Xu G, Zhao Y, Hoffman C M, Lin H, Torchinsky D H, Broholm C L, Bansil A and Tafti F 2020 arXiv:2006.07943 [cond-mat.mtrl-sci]
[28] Lyu M, Xiang J, Mi Z, Zhao H, Wang Z, Liu E, Chen G, Ren Z, Li G and Sun P 2020 *Phys. Rev. B* **102** 085143
[29] Bobev S, Tobash P H, Fritsch V, Thompson J D, Hundley M F, Sarrao J L and Fisk Z 2005 *J. Solid State Chem.* **178** 2091
[30] Dhar S K, Pattalwar S M and Vijayaraghavan R 1992 *J. Magn. Magn. Mater.* **104–107** 1303
[31] Dhar S K and Pattalwar S M 1996 *J. Magn. Magn. Mater.* **152** 22
[32] Cardinale A M and Parodi N 2018 *J. Therm. Anal. Calorim.* **134** 1327
[33] Cardinale A, Macciò D and Saccone A 2015 *J. Therm. Anal. Calorim.* **121** 1151
[34] Yang S, Guo Y and Wang C 2019 *Phys. Status Solidi B* **257** 1900141
[35] Jung M H, Park S H, Kim H C and Kwon Y S 2004 *J. Magn. Magn. Mater. Suppl.* **272–276** E431
[36] Destraz D, Das L, Tsirkin S S, Xu Y, Neupert T, Chang J, Schilling A, Grushin A G, Kohlbrecher J, Keller L, Puphal P, Pomjakushina E and White J S 2020 *npj Quantum Mater.* **5** 5
[37] Higashinaka R, Yamada A, Matsuda T D and Aoki Y 2018 *AIP Adv.* **8** 125017
[38] Williams D S, Shand P M, Pekarek T M, Skomski R, Petkov V and Leslie-Pelecky D L 2003 *Phys. Rev. B* **68** 214404
[39] Baran S, Przewoźnik J, Kalychak Y M, Tyvanchuk Y and Szytuła A 2016 *J. Magn. Magn. Mater.* **410** 156
[40] Tyvanchuk Y B, Szytuła A, Zarzycki A, Rodewald U C, Kalychak Y M and Pöttgen R 2008 *J. Solid State Chem.* **181** 3223
[41] Jesus C B R, Piva M M, Rosa P F S, Adriano C, Fisk Z and Pagliuso P G 2015 *Phys. Procedia.* **75** 618
[42] Hase M, Soda M, Masuda T, Kawana D, Yokoo T, Itoh S, Matsuo A, Kindo K and Kohno M 2014 *Phys. Rev. B* **90** 024416
[43] Nickerson J C, White R M, Lee K N, Bachmann R, Geballe T H and Hull G W 1971 *Phys. Rev. B* **3** 2030
[44] Mendpara H, Joshi D A, Nigam A K and Thamizhavel A 2015 *J. Magn. Magn. Mater.* **377** 325
[45] Tamura R, Muro Y, Hiroto T, Yaguchi H, Beutier G and Takabatake T 2012 *Phys. Rev. B* **85** 014203
[46] He Q and Guo Y 2016 *Appl. Phys. A* **122** 455
[47] Chen S, Guo Y and He Q 2015 *J. Appl. Phys.* **117** 123910
[48] Yakushiji K, Mitani S, Takanashi K, Ha J G and Fujimori H 2000 *J. Magn. Magn. Mater.* **212** 75